Radiation-induced polymerization of 3-hexylthiophene in oxygen-free and oxygen-saturated dichloromethane solvent

Teseer Bahry [a], Zhenpeng Cui [a], Alexandre Dazzi [a], Matthieu Gervais [b], Cyrille Sollogoub [b], Fabrice Goubard [c], Thanh-Tuân Bui [c], Samy Remita [a,d,*]

[a] Institut de Chimie Physique, ICP, UMR 8000, CNRS, Université Paris-Saclay, Bâtiment 349, Campus d'Orsay, 15 Avenue Jean Perrin, 91405, Orsay Cedex, France
[b] Laboratoire PIMM, Arts et Métiers Institute of Technology, CNRS, CNAM, Hesam Université, F-75013, Paris Cedex, France
[c] CY Cergy Paris Université, LPPI, F95000, Cergy, France
[d] Département Chimie Vivant Santé, EPN 7, Conservatoire National des Arts et Métiers, CNAM, 292 Rue Saint-Martin, 75141, Paris Cedex 03, France

Keywords:
Radiolysis
Conducting polymers
Poly(3-hexylthiophene)
P3HT

A B S T R A C T

As alternative radiolytic approach, the synthesis of P3HT was made possible thanks to the oxidation of 3HT monomers by chloromethyl and dichloromethyl radicals or by their corresponding peroxyl radicals *in situ* produced by dichloromethane solvent radiolysis. Under two different experimental conditions, in oxygen-free solution and in oxygen-saturated solution, two different polymers, "$P3HT_{N_2}$" and "$P3HT_{O_2}$" respectively, were successfully synthesized. Both produced materials were discerned by several analytical and spectroscopic techniques. UV–Vis absorption spectroscopy results showed that the radiolytic yield of 3HT oxidation in dichloromethane solvent is higher under O_2 atmosphere. Indeed, a dose of 75 kGy was needed to polymerize 10 mM in 3HT under N_2 atmosphere, meanwhile a dose of 35 kGy was sufficient to polymerize the same amount of 3HT under O_2. The average molecular weight of $P3HT_{O_2}$ was found higher than that of $P3HT_{N_2}$ as revealed by SEC chromatography analysis. Also, $P3HT_{O_2}$ exhibits better thermal stability than $P3HT_{N_2}$. ATR-FTIR spectroscopy revealed the specific presence into $P3HT_{O_2}$ polymers of some functional groups such as carbonyl, hydroxyl and carboxyl moieties, which clearly explains the difference between the morphological structures of $P3HT_{N_2}$ and $P3HT_{O_2}$ as highlighted by cryo-TEM, SEM and AFM microscopies. Finally, both radio-synthesized $P3HT_{N_2}$ and $P3HT_{O_2}$ polymers were found characterized by remarkably significant conductive, electronic and optical properties.

1. Introduction

Poly (3-hexylthiophene), P3HT, is considered as the best candidate for organic photovoltaic devices, due to its remarkable optical and conductive properties (Murali et al., 2015; Tremel and Ludwigs, 2014). P3HT exhibits good thermal stability, high processability, synthetic versatility and susceptibility to tune and change its properties and morphology through simple ring modifications (Marrocchi et al., 2012). P3HT is basically synthesized through oxidative polymerization of 3-hexylthiophene (3HT) monomers, which are in the preliminary step oxidized into their radical cations (Jiang et al., 2012). The formation of these radical cations and the subsequent polymerization into P3HT is realizable by several oxidation routes: the most common ways being the chemical and electrochemical approaches (Brooke et al., 2017).

The importance of P3HT-based materials highly motivated and still motivates scientific community to discover new alternative synthesis ways (Brooke et al., 2017). Between the new potential alternative routes, ionizing radiation-induced polymerization by γ-rays, which does not involve any external oxidizing agent, appears to be a very promising and easy way to produce different kinds of conducting polymers, such as P3HT. Indeed, this radiolytic method is now well exploited in order to synthesize nanostructured conducting polymers in aqueous solutions (Cui et al., 2014; Lattach et al., 2013, 2014). A variety of nanostructured conducting polymers (e.g. PEDOT, PPy and PTAA) were effectively obtained by 3,4-ethylenedioxythiophene (EDOT), pyrrole (Py) and 3-thiophene acetic acid (TAA) monomer oxidation by using different oxidizing species *in situ* produced by aqueous solution radiolysis: hydroxyl radicals ($HO^{\bullet}$) (Coletta et al., 2015; Cui et al., 2014, 2017; Lattach et al., 2013),

* Corresponding author. Institut de Chimie Physique, ICP, UMR 8000, CNRS, Université Paris-Saclay, bâtiment 349, Campus d'Orsay, 15 avenue Jean Perrin, 91405, Orsay Cedex, France.
E-mail address: samy.remita@universite-paris-saclay.fr (S. Remita).

dichloride radical anions ($Cl_2^{\bullet-}$) (Cui et al., 2019), azide radicals ($N_3^{\bullet}$) (Lattach et al., 2014) or sulfate radicals ($SO_4^{\bullet-}$) (Coletta et al., 2016). This method was further developed to produce PEDOT conducting polymers by reduction method by using hydrated electrons (e_{aq}^-) also generated by water radiolysis (Cui et al., 2016). However, this radiolytic approach is not totally achievable and not extendable to P3HT polymers due to the fact that 3HT monomers are completely insoluble in aqueous solutions.

As demonstrated in previous works, γ-radiolysis of dichloromethane is potentially pertinent as an alternative radiolytic approach for the production of conducting polymers by the way of monomer oxidation. Indeed, radiolysis of deaerated solutions of dichloromethane first generates solvated electrons in addition to chloride radicals and dichloromethane radical cations which quickly lead to two main species: chloromethyl ($^{\bullet}CH_2Cl$) and dichloromethyl ($^{\bullet}CHCl_2$) radicals, which both are known as oxidizing agents (Alfassi et al., 1989; Emmi et al., 1999). This alternative approach in deaerated dichloromethane solutions enabled the successful oxidation of EDOT and TAA monomers and the production of PEDOT as well as PTAA conducting polymers (Bahry et al., 2018); (Bahry et al., 2020). Similar radiolytic approach was also performed in other organic solvents such as chloroform, hexane and neat monomer solution in order to initiate the oxidative polymerization of 3-octylthiophene (3OT) (Ishigaki and Koizumi, 2012). However, even if chloromethyl ($^{\bullet}CH_2Cl$) and dichloromethyl ($^{\bullet}CHCl_2$) radicals have already been used as oxidizing species, their redox potentials are not so high (Emmi et al., 1989, 1999). Thus, this radiolytic approach in deaerated dichloromethane solution could be problematic in case of organic monomers possessing high oxidation potentials, such as 3HT monomers which are characterized by an oxidation potential ~1.84 V_{SCE} (Cutler, 2000; Roncali et al., 1987) (Cutler, 2000; Ferraris and Newton, 1992; Wei et al., 1991), much higher than that of EDOT monomers (1.40 V_{SCE}) (Lattach et al., 2013).

Interestingly, when dichloromethane solutions are irradiated in presence of oxygen (in aerated or oxygen-saturated conditions), the produced chloromethyl and dichloromethyl radicals are rapidly scavenged by dissolved molecular oxygen (O_2) producing the corresponding peroxyl radicals: $CH_2ClO_2^{\bullet}$ and $CHCl_2O_2^{\bullet}$. These latter are known as strong oxidizing agents towards organic materials, their redox potentials being much higher than those of chloromethyl ($^{\bullet}CH_2Cl$) and dichloromethyl ($^{\bullet}CHCl_2$) radicals (Alfassi et al., 1989; Emmi et al., 1989, 1999). By means of $CH_2ClO_2^{\bullet}$ and $CHCl_2O_2^{\bullet}$ peroxyl radicals, one can thus consider, in aerated or oxygen-saturated solutions of dichloromethane, a higher yield of monomer oxidation as well as a greater efficiency of polymerization.

In the present work, starting from 3HT monomers which are completely insoluble in water and which are characterized by a very high redox potential, the challenge was to efficiently synthesize by means of gamma-radiolysis and for the first time in literature, nanostructured P3HT conducting polymers within dichloromethane solvent. Polymerization of 3HT into P3HT was thus conducted by following two routes: first in an oxygen-free solution ($P3HT_{N_2}$) and second in an oxygen-saturated solution ($P3HT_{O_2}$) of dichloromethane (Scheme 1).

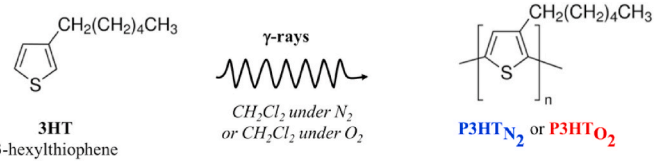

Scheme 1. Radiation-induced polymerization of 3-hexylthiophene (3HT) in dichloromethane solvent under N_2 and O_2 atmospheres.

2. Experimental

2.1. Reagents and solvents

3-hexylthiophene, 3HT (99% purity), was purchased from Sigma-Aldrich and used as a monomer. Dichloromethane (DCM) anhydrous (≥99.8%), acetonitrile (ACN) (≥99.9%) and the other used solvents were purchased from Sigma-Aldrich. Distilled water (Millipore system 18.2 Ω cm^{-1}) was used for washing. Nitrogen (N_2) and oxygen (O_2) (from Air Liquid Co. with purity 99.99%) were respectively used to deaerate or to saturate with oxygen dichloromethane solutions before γ-irradiations. Tetrabutylammonium hexafluorophosphate, $TBAPF_6$ (as electrolyte), and Ferrocene (bis(cyclopentadienyl)iron, di (cyclopentadienyl)iron), Fc (as standard), were used for electrochemical measurements. Nitrosyl tetrafluoroborate ($NOBF_4$) (≥95%, Sigma-Aldrich) dissolved in acetonitrile was used as dopant during the electrical conductivity measurements. All compounds were used as received. All experiments were performed at room temperature.

2.2. Solutions preparation

Dichloromethane solutions containing 10 mM in 3HT monomers were prepared at ambient temperature. Note that the used concentration is lower than 3HT solubility in dichloromethane at 25 °C, which is more than 50 mM as found by UV–Vis absorption spectroscopy study (results not shown). This concentration also remains much lower than dichloromethane molecules concentration (15.6 M). This enables one to neglect the direct effect of ionizing radiation on 3HT monomers. Dichloromethane solutions were degassed with N_2 or O_2 for 20 min and were then sealed in glass ampoules. The solutions were finally irradiated with a ^{60}Co γ-source with increasing doses up to 140 kGy at a dose rate of 4.1 kGy h^{-1}.

2.3. Radiation-induced synthesis of $P3HT_{N_2}$ and $P3HT_{O_2}$

Dichloromethane radiolysis under N_2. Under these experimental conditions, solvated electrons, chloride radicals, $Cl^{\bullet}$, and dichloromethane radical cations, $CH_2Cl_2^{\bullet+}$, which are first produced from solvent molecules, quickly lead to two main reactive species: chloromethyl ($^{\bullet}CH_2Cl$) and dichloromethyl ($^{\bullet}CHCl_2$) radicals (Alfassi et al., 1989; Emmi et al., 1989, 1999) according to:

$$CH_2Cl_2 \rightarrow [e^- + Cl^{\bullet} + CH_2Cl_2^{\bullet+}] \rightarrow {}^{\bullet}CHCl_2 + CH_2Cl^{\bullet} + HCl \quad (1)$$

Those reactive species are capable to generate radical cations of many organic compounds (Alfassi et al., 1989; Ushida et al., 1999), such as thiophenes and oligothiophenes ($Th^{\bullet+}$) (Emmi et al., 1999). Besides, it was well established in previous studies that gamma-induced polymerization of two thiophene derivatives, namely EDOT and TAA monomers, in dichloromethane solvent under N_2 atmosphere, can be initiated by the generated $^{\bullet}CH_2Cl$ and $^{\bullet}CHCl_2$ oxidizing radicals (Bahry et al., 2018, 2020). One can thus assume that these two species will also be able to initiate the oxidative polymerization of 3HT in the same experimental conditions. The oxidation of EDOT and TAA monomers was made possible since their ionization potentials are low enough (~4.2 eV) (Bahry et al., 2018, 2020; Lattach et al., 2013). Due to these low potentials, the yield of monomers (EDOT or TAA) oxidation, G_{ox}, was found equal to 4.12×10^{-7} mol J^{-1} in both cases. Also, irradiation dose, D_{max}, needed for quantitative polymerization of 10 mM in either EDOT or TAA monomers was found equal to 36 kGy. Indeed, D_{max} is related to G_{ox} by the following equation (Bahry et al., 2018, 2020):

$$D_{max}(Gy) = \frac{2\,[Monomers]_0\ (mol.L^{-1})}{G_{ox}\ (mol.J^{-1}) \times d\ (kg.L^{-1})} \quad (2)$$

where $[Monomers]_0$ is the initial concentration in organic monomers and where d is dichloromethane density (d = 1.35 kg L^{-1}).

Nevertheless, since 3-alkylthiophene derivatives, such as 3HT, possess higher oxidation potentials than those of EDOT and TAA (Roncali et al., 1987), one can expect that the yield of 3HT oxidation in dichloromethane solvent under N_2 atmosphere, will be lower than 4.12 $\times$ 10^{-7} mol J^{-1}, while the dose, D_{max}, needed for quantitative polymerization of 10 mM in 3HT (optimized formation of $(P3HT_{N_2})$) will be higher than 36 kGy according to equation (2).

To verify the value of D_{max} needed for quantitative polymerization of 3HT, a dose effect study was carried out in dichloromethane solvent under N_2 atmosphere. In this context, solutions of dichloromethane containing 10 mM in 3HT were prepared under N_2 by degassing the samples for 20 min in sealed glass ampoules at ambient temperature. The solutions were then irradiated with γ-rays at doses ranging from 15 to 140 kGy.

Dichloromethane radiolysis under O_2. In O_2-saturated solutions of dichloromethane, the produced chloromethyl ($^{\bullet}CH_2Cl$) and dichloromethyl ($^{\bullet}CHCl_2$) radicals are rapidly scavenged by O_2 molecules leading to the corresponding peroxyl radicals: $CH_2ClO_2^{\bullet}$ and $CHCl_2O_2^{\bullet}$ (Alfassi et al., 1989; Emmi et al., 1999), according to:

$$^{\bullet}R\ Cl + O_2 \rightarrow RClOO^{\bullet} \quad (3)$$

Peroxyl radicals possess much higher oxidizing power with respect to original carbon centered radicals. Peroxyl radicals are thus capable to oxidize many kinds of organic compounds (Alfassi et al., 1989). Introducing oxygen in dichloromethane solutions containing thiophene and oligothiophene molecules was shown to facilitate their oxidation, as highlighted by pulse radiolysis experiments performed in aerated and deaerated solutions of dichloromethane (Emmi et al., 1999, 2003). Alfassi et al. evaluated by pulse radiolysis the total yield of oxidation of various organic solutes by peroxyl radicals produced by radiolysis of aerated dichloromethane solutions. It was shown, dependently on solute concentration, that the total yield of oxidation by the primary radicals and the peroxyl radicals amounts to 7.77 $\times$ 10^{-7} mol J^{-1} (Alfassi et al., 1989). Even if this total yield of oxidation has been specifically evaluated in aerated dichloromethane solution, one can suppose that the total yield of oxidation in an oxygen-saturated dichloromethane solution is not so far from 7.77 $\times$ 10^{-7} mol J^{-1}. Once again, since 3HT monomers possess high oxidation potential, one can expect that the total yield of 3HT oxidation in dichloromethane solvent under O_2 atmosphere, will be lower than 7.77 $\times$ 10^{-7} mol J^{-1}, while the dose, D_{max}, needed for quantitative polymerization of 10 mM in 3HT (optimized formation of $(P3HT_{O_2})$) will be higher than 19 kGy according to equation (2).

To check the value of D_{max} needed for quantitative polymerization of 3HT in these experimental conditions, a dose effect study was carried out in dichloromethane solvent, this time under oxygen atmosphere. Solutions of dichloromethane containing 10 mM in 3HT were prepared under O_2 by degassing the samples for 20 min in sealed glass ampoules at ambient temperature. The solutions were then irradiated with γ-rays at doses ranging from 15 to 55 kGy.

Polymers post-treatment. In order to evaporate the solvent and to extract $P3HT_{N_2}$ and $P3HT_{O_2}$ polymers after gamma irradiation, a rotary evaporator was used. After solvent evaporation brownish glutinous polymers were obtained. These materials were then used for many characterizations and spectral analysis.

2.4. Characterization methods

- **UV–Vis absorption spectroscopy.** UV–Vis absorption spectroscopy was used to check the optical properties of 3HT monomers and those of $P3HT_{N_2}$ and $P3HT_{O_2}$ polymers radiosynthesized in dichloromethane at increasing doses, respectively under N_2 and O_2 atmospheres. For this purpose, after gamma-irradiation and after post-treatment, glutinous $P3HT_{N_2}$ and $P3HT_{O_2}$ polymer powders were dissolved in 1 mL DCM. The spectra of the obtained solutions were then recorded on a HP 8543 spectrophotometer.
- **Size exclusion chromatography (SEC).** SEC was used in order to check the average molecular weight of $P3HT_{N_2}$ and $P3HT_{O_2}$ polymers. For this purpose, 10 mg of glutinous $P3HT_{N_2}$ and $P3HT_{O_2}$ polymers obtained after dichloromethane evaporation were dissolved in 1 mL THF. Then 100 μL of each THF solution was injected into SEC apparatus. Using THF as eluent, SEC was performed at 40 °C on a Malvern Viscotek TDA apparatus equipped with two columns, Malvern T3000 and T6000, with a Malvern refractive index detector at an elution rate of 1 mL min^{-1}. Polystyrene polymers were used as standards.
- **Attenuated Total Reflectance Fourier Transform Infrared (ATR-FTIR) spectroscopy.** FTIR was used for chemical characterization of radiosynthesized $P3HT_{N_2}$ and $P3HT_{O_2}$ polymers. The dried polymers were deposited and squeezed on the ATR support of the FTIR spectrophotometer. Measurements were recorded by using a Bruker Vertex 70 FTIR spectrophotometer and conducted as in previous work ((Bahry et al., 2020).
- **Thermogravimetric (TGA) analysis.** Thermal stability and composition analysis of $P3HT_{N_2}$ and $P3HT_{O_2}$ polymers synthesized in dichloromethane were performed on a thermogravimetric analysis instrument TGA Q500 (TA Instruments, USA) under a nitrogen flow of 50 mL min^{-1}. To this end, few mg of dried $P3HT_{N_2}$ and $P3HT_{O_2}$ polymer powders were used. The temperature ranged from 25 to 800 °C at a heating rate of 10 °C min^{-1}.
- **Cryogenic-transmission electron microscopy (Cryo-TEM).** In order to check the morphology of $P3HT_{N_2}$ and $P3HT_{O_2}$ polymers dispersed in dichloromethane, cryo-TEM microscopy was used. For this purpose, 10 mg of glutinous $P3HT_{N_2}$ and $P3HT_{O_2}$ polymers obtained after post-treatment and dichloromethane evaporation were dissolved in 1 mL DCM. A drop of each prepared solution, containing $P3HT_{N_2}$ or $P3HT_{O_2}$, was then deposited on "quantifoil" holey-carbon-coated grids and quench-frozen by being rapidly plunged into liquid ethane. The observations were carried out on a transmission electron microscope LaB6 JEOL JEM 2100 (JEOL, Japan) operating at 200 kV in a cryogenic environment (Cryo-TEM). The experimental procedure is the same as that already described in previous work ((Bahry et al., 2020).
- **Scanning Electron Microscopy (SEM) and Energy-dispersive X-ray spectroscopy (EDX).** In order to investigate the structure of radiosynthesized $P3HT_{N_2}$ and $P3HT_{O_2}$ polymers and to check their morphology after deposition, the dried polymer powders obtained after post-treatment and dichloromethane evaporation were sprinkled onto carbon tape adhered to aluminum mounts and then coated with gold in order to get high imaging resolution. The SEM observations were performed by using an EVO MA 10 ZEISS microscope as already described ((Bahry et al., 2020). *In situ* EDX was carried out without gold coating to identify the chemical composition of the materials and to perform their elemental analysis.
- **Atomic Force Microscopy (AFM).** AFM was used to check the topographical morphology of $P3HT_{N_2}$ and $P3HT_{O_2}$ polymers. In this context, 3 mg of dried polymer powders were solubilized in 1 mL of ethanol. A small drop of each ethanolic solution was then deposited onto mica sheet and dried naturally. The AFM (nanoIR, Anasys Instruments Corp, Bruker NANO Group, California, USA) was used in tapping mode as previously described ((Bahry et al., 2020).
- **Electrical conductivity measurements by four-point probe technique.** Four-point probe technique was used to measure the conductivity of $P3HT_{N_2}$ and $P3HT_{O_2}$ polymers. In this context, the dried polymer powders obtained after post-treatment and dichloromethane evaporation were dissolved in DCM at a concentration of 10 mg mL^{-1}. Then, 100 μL of each solution were spin-coated on clean glass substrate at a speed of 100 rpm for 60 s. Afterwards, the obtained films were rinsed and doped with $NOBF_4$ at a concentration of 20 mM in acetonitrile. The substrates were then placed on a hot plate and heated up to 130 °C for 30 min in order to dry and evaporate the remaining solvent. After measuring the thickness of the films by a 3

T. Veeco Dektak 150 surface profiler, their resistance was determined by a Kelvin four-point probe technique. The conductivities, ρ (S cm^{-1}), of $P3HT_{N_2}$ and $P3HT_{O_2}$ films were finally determined as previously explained (Bahry et al., 2020).

Cyclic-voltammetry measurements (CV). Cyclic voltammetry (CV) was used in order to investigate the electrochemical properties and to determine the electronic band gaps of $P3HT_{N_2}$ and $P3HT_{O_2}$ polymers. The electrochemical setup was a three-electrodes cell made of Pt disc as working electrode, an Au wire as counter-electrode and an Ag/AgCl wire as pseudo-reference electrode. Calibration of pseudo-reference electrode was ensured by probing ferrocenium/ferrocene (Fc^+/Fc) redox potential measured at the end of each experiment, as recommended by IUPAC (Gritzner and Kuta, 1984). $P3HT_{N_2}$ and $P3HT_{O_2}$ polymers obtained after post-treatment and dichloromethane evaporation were dissolved in DCM solution at a concentration of 1 mg mL^{-1}. Then, 1 mL of each solution was mixed into the electrochemical cell with 5 mL of acetonitrile solution con-taining tetrabutylammonium hexafluorophosphate ($TBAPF_6$) used as electrolyte at a concentration of 0.1 M. The three electrodes were then immersed into the electrochemical cell and the cyclic voltam-mograms were recorded at a scan rate of 20 mV s^{-1} between − 2.5 V and +2.5 V.

Results and discussion

3.1. Spectral analysis of 3HT-containing irradiated solutions

Dichloromethane solution containing 10 mM in 3HT appears colorless before irradiation (insert of Fig. 1a). Also, its absorption spectrum is displayed in Fig. 1a. As observed 3HT is characterized by a maximal absorption at 238 nm. This is in good agreement with literature since thiophene molecules are known to absorb light in the UV-region between 225 nm and 245 nm, this absorption being ascribed to π-π* transition (Beiting et al., 1985). The study of the variation of 3HT absorption as a function of its concentration in dichloromethane enabled us to find that 3HT is soluble up to 50 mM. Also, using Beer-Lambert's law (results not shown), the extinction coefficient at 238 nm was found to be $\varepsilon_{238} = 5570$ L mol^{-1} cm^{-1}.

3.1.1. Dose effect study under N_2 and O_2 atmospheres

Due to the knowledge of extinction coefficient values of dissolved monomers, it should be possible to follow the variation of 3HT concentration as a function of the irradiation dose and then to deduce the initial radiolytic yield of 3HT oxidation (Lattach et al., 2013). Unfortunately, this is not possible when considering dichloromethane radiolysis. Indeed, gamma-irradiation of dichloromethane leads to the generation of several transient species and stable products, such as (1, 1-dichloroethane, 1,2-dichloroethane, 1,1,2-trichloroethane and 1,1,2, 2-tetrachloroethane), which absorb light in the wavelength range 230–400 nm (Truszkowski and Szymański, 1994), causing an overlap with the absorption of 3HT as already observed in case of EDOT monomers (Bahry et al., 2018, 2020). Thus, in the present experimental conditions in dichloromethane solvent, it is not possible to determine in this way the initial radiolytic yield of 3HT oxidation, G_{ox}, nor the irradiation dose, D_{max}, needed for quantitative polymerization of 10 mM in 3HT monomers according to equation (2).

Nevertheless, as previously highlighted in previous works, it is possible to evaluate the approximate irradiation dose needed to achieve the complete oxidative polymerization of dissolved monomers by following the UV–Vis absorption spectra of the produced polymers as a function of the irradiation dose (Bahry et al., 2018, 2020). Accordingly, solutions of dichloromethane under either N_2 or O_2 atmospheres and containing 10 mM in 3HT were irradiated at increasing doses from 15 to 140 kGy. The glutinous $P3HT_{N_2}$ and $P3HT_{O_2}$ polymer powders obtained in each case after post-treatment were then redissolved in 1 mL DCM. The color gradations of the resulting solutions are presented in

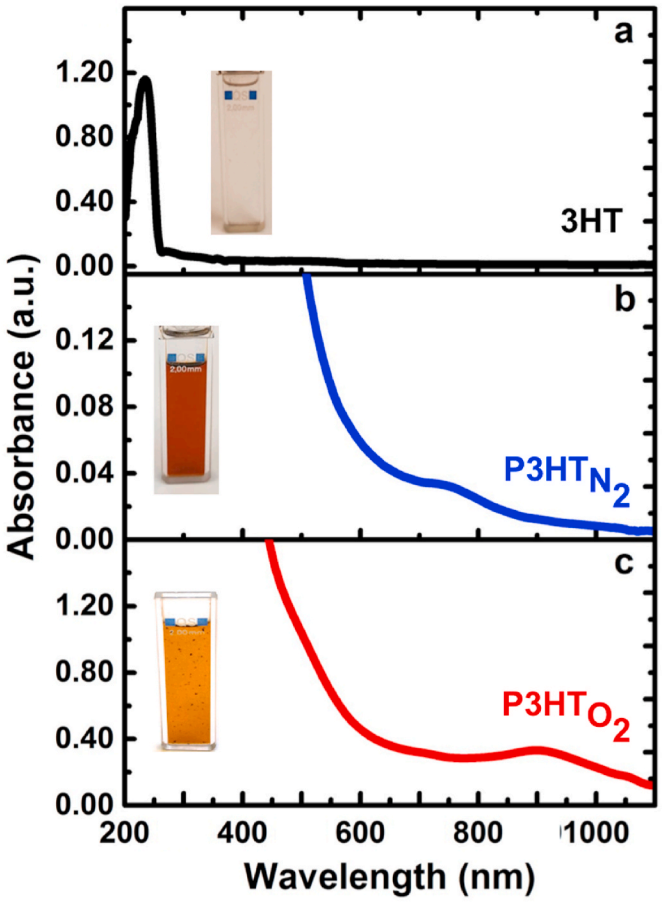

Fig. 1. UV–Vis absorption spectra of dichloromethane solutions containing 10 mM in 3HT: a) non-irradiated and diluted 10 times b) irradiated under N_2 atmosphere at 75 kGy (formation of $P3HT_{N_2}$) c) irradiated under O_2 atmosphere at 35 kGy (formation of $P3HT_{O_2}$). Spectra b) and c) were recorded after extraction and redissolution of radiosynthesized polymers in 1 mL DCM. Reference was pure solvent. L = 0.2 cm. Inserts: photographs of the three dichloromethane solutions.

Supplementary Information (Figure S.I.1). The corresponding UV–visible absorption spectra were also recorded as a function of the absorbed dose as displayed in Supplementary Information (Figure S.I.2). As observed, processing the solutions with irradiation doses higher than 75 kGy under N_2 or higher than 35 kGy under O_2, leads to a gradual decrease in the absorption, around 750 nm under N_2 and around 900 nm under O_2, which will be later attributed to $P3HT_{N_2}$ and $P3HT_{O_2}$ respectively.

According to literature (Bahry et al., 2018, 2020), these spectral variations above these two doses indicate the occurrence of damage, degradation and breaking down of the polymer chains due to over-oxidation. Thus, this dose effect study on 3HT monomers dissolved in dichloromethane, enabled the determination of the approximate irradiation doses, D_{max}, needed for quantitative polymerization of 10 mM in 3HT monomers either under N_2 atmosphere (75 kGy) or under O_2 atmosphere (35 kGy). As observed, introducing oxygen into dichloromethane solutions reduces the irradiation dose needed for quantitative polymerization of 3HT. The fact that D_{max} is lower under O_2 atmosphere than under N_2 atmosphere means that the yield of 3HT oxidation is higher in the presence of oxygen as expected. Indeed, this is due to the higher oxidation potentials of $CH_2ClO_2^{\bullet}$ and $CHCl_2O_2^{\bullet}$ peroxyl radicals produced under O_2 in comparison with those of chloromethyl ($^{\bullet}CH_2Cl$) and dichloromethyl ($^{\bullet}CHCl_2$) radicals produced under N_2. As far as we can discern, halogenated alkyl peroxyl radicals boost the oxidative

polymerization and therefore facilitate the formation of P3HT polymers. In contrast, the oxidation of 3HT by the original carbon centered radicals is difficult to achieve unless one delivers relatively high irradiation dose.

In dichloromethane solvent under N_2 atmosphere, the fact that D_{max} is found higher than 36 kGy (see section 2.3) means that the yield of 3HT oxidation, G_{ox}, is lower than 4.12×10^{-7} mol J^{-1} according to equation (2). In the same way, in dichloromethane solvent under O_2 atmosphere, a D_{max} value higher than 19 kGy (see once again section 2.3) implies a yield of 3HT oxidation lower than 7.77×10^{-7} mol J^{-1}. These relatively low yields of 3HT oxidation found either under nitrogen or under oxygen are in very good agreement with the well-known high redox potential of 3HT monomers (Emmi et al., 1989; Isse et al., 2011; Roncali et al., 1987; Ushida et al., 1999).

3.1.2. Radiation-induced synthesis of $P3HT_{N_2}$ polymers at 75 kGy under N_2

According to the dose effect study, the complete and optimal $P3HT_{N_2}$ production in dichloromethane solvent under N_2 atmosphere is attained at around 75 kGy. The UV–Vis absorption spectrum of $P3HT_{N_2}$ polymers produced at 75 kGy is displayed in Fig. 1b. The solution which was colorless before irradiation (insert of Fig. 1a) transformed to brownish at this absorbed dose as exhibited in insert of Fig. 1b. Note that the solution appears homogeneous reflecting the relatively high solubility of $P3HT_{N_2}$ materials in DCM solvent.

The absorption spectrum in Fig. 1b displays an absorption band at 750 nm, which is attributed to the formation of $P3HT_{N_2}$ polymers and ascribed to the π-π* transition along the polymer chains (Ishigaki and Koizumi, 2012). The red-shifted absorption at 750 nm corresponds to polaron and/or bipolaron bands, originating from the oxidized state of doped $P3HT_{N_2}$ polymers ((Bahry et al., 2018; Kim et al., 2009). Indeed, as highlighted in previous works, dichloromethane radiolysis generates chloride ions which enable the *in situ* production of doped polymers (Bahry et al., 2018, 2020)). In the same way, $P3HT_{N_2}$ polymers should be produced in the present work doped with chloride ions. This will be further demonstrated.

3.1.3. Radiation-induced synthesis of $P3HT_{O_2}$ polymers at 35 kGy under O_2

One can extrapolate from the dose effect study that the dose needed for complete and optimal synthesis of $P3HT_{O_2}$ in dichloromethane solvent under O_2 atmosphere occurs at around 35 kGy. The UV–Vis absorption spectrum of $P3HT_{O_2}$ polymers radiosynthesized at this irradiation dose is presented in Fig. 1c. Yellowish solution with suspended particles was obtained at this optimal absorbed dose as observed in insert of Fig. 1c. These particles will be later identified as aggregated hydrophilic $P3HT_{O_2}$ materials.

It is possible to see from $P3HT_{O_2}$ spectrum a slight shoulder at 500 nm (see also Figure S.I.2) together with a more or less prominent peak at 900 nm. The shoulder at 500 nm, originating from π-π* transitions along the polymer chains, is attributed to the formation of $P3HT_{O_2}$ polymers (Ishigaki and Koizumi, 2012). The peak at 900 nm is attributed to polaron and/or bipolaron bands, which are characteristic of doped polymers (Bahry et al., 2018; Kim et al., 2009). Indeed, as in case of $P3HT_{N_2}$ polymers produced in dichloromethane under nitrogen, $P3HT_{O_2}$ polymers produced in the same solvent but under oxygen should be found doped with chloride ions generated by DCM radiolysis. This will also be further demonstrated.

3.1.4. A comparison between $P3HT_{N_2}$ and $P3HT_{O_2}$ absorption spectra

By comparing spectra of Fig. 1b and c (both recorded after dissolution of radiosynthesized polymer powders in 1 mL DCM), one can observe that spectral features of $P3HT_{O_2}$ are clearly more prominent than those observed in case of $P3HT_{N_2}$. The absorption intensity is higher in case of $P3HT_{O_2}$. Also, the doping band of polymers produced in dichloromethane is shifted from 750 nm in case of $P3HT_{N_2}$ to 900 nm in case of $P3HT_{O_2}$.

As it will be later demonstrated by SEC analysis, this red-shift is attributed to the formation of P3HT polymers possessing higher molecular weight. In addition, the shift to higher wavelengths also might be originated from the formation of P3HT polymers with head to tail pattern. This red shift is commonly observed in case of regioregular configuration due to the increase of the conjugation along the polymer chains. The blue shift which is in turn obtained in case of regiorandom pattern causes decrease in the conjugation. This decrease comes from the twisting of the thiophene ring and from the lower number of π-π stacking interactions along the polymers (Barta et al., 1999; Cutler, 2000; Mccullough et al., 1993; Pappenfus et al., 2010).

3.2. Molecular weight analysis of $P3HT_{N_2}$ and $P3HT_{O_2}$ polymers

To estimate the molecular weights of $P3HT_{N_2}$ and $P3HT_{O_2}$ polymers and to check whether the atmosphere has an influence on the degree of polymerization, SEC was performed on the polymers which were produced at the optimal irradiation doses, D_{max}, enabling quantitative polymerization: 75 kGy for $P3HT_{N_2}$ and 35 kGy for $P3HT_{O_2}$. Both samples were analyzed by dissolving in THF the glutinous solid parts that were obtained after dichloromethane solvent evaporation (Scheme 2). The photographs of the obtained THF solutions are displayed in insert of Fig. 2.

The obtained SEC chromatograms are shown in Fig. 2 and the molar masses of P3HT polymers, obtained with a polystyrene calibration at M_p (the peak molecular weight, that is to say the mass at the maximum of highest peak in each chromatogram), are reported in the inserted table of Fig. 2. From the chromatogram of $P3HT_{N_2}$, it was possible to extrapolate the molar mass (M_p) of 1785 g mol^{-1} with a polydispersity index of 1.22. This molar mass corresponds in case of $P3HT_{N_2}$ to about 10 units of 3HT monomers per polymer chain. This molecular weight implies that the polymerization of 3HT under N_2 produces regiorandom P3HT oligomers. This relatively low degree of polymerization has already been reported in literature for regio-irregular poly (3-alkythiophenes) (Barta et al., 1999). Interestingly, one can also detect in $P3HT_{N_2}$ chromatogram the presence of polymers with higher molecular weight. In particular, the weight average molecular weight (M_w) is equal to 3042 g mol^{-1}, which corresponds to about 18 units of 3HT per polymer chain. Besides, from the chromatogram of $P3HT_{O_2}$, it was possible to extrapolate the molar mass (Mp) of 3150 g mol^{-1} with a polydispersity index of 1.25. In case of $P3HT_{O_2}$ polymers, the obtained molar mass corresponds to about 18 units of 3HT per polymer chain. As it will be later demonstrated by ATR-FTIR spectroscopy, $P3HT_{O_2}$ polymers are functionalized with carbonyl and hydroxyl groups. However, since the number of functional groups and their distribution along $P3HT_{O_2}$ polymers are not known, those groups are not taken into account for the evaluation of the degree of polymerization. Also, in case of $P3HT_{O_2}$, the weight average molecular weight (M_w) is found equal to 4800 g mol^{-1} (28 units of 3HT per polymer chain) highlighting the presence in the sample of polymers with more longer chain lengths. Since $P3HT_{O_2}$ polymers possess longer chain lengths than $P3HT_{N_2}$ ones, $P3HT_{O_2}$ materials should be characterized by a higher degree of

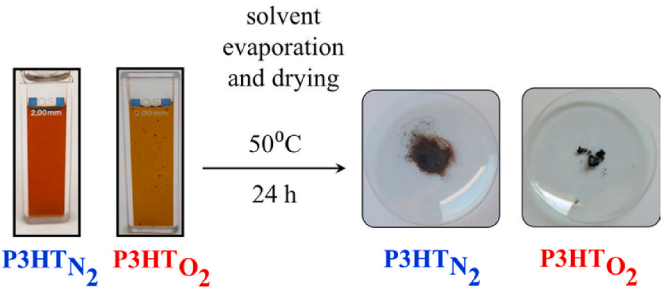

Scheme 2. The post processing of P3HT polymers after gamma-irradiation.

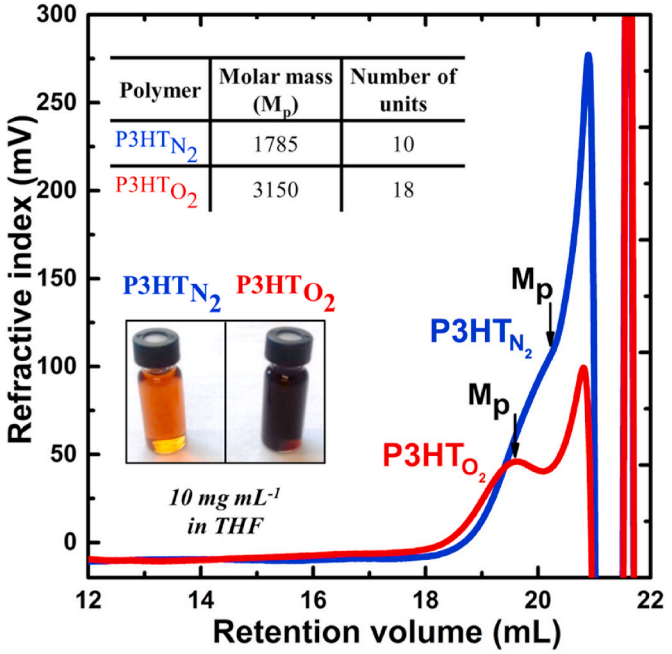

Fig. 2. SEC chromatograms of 10 mg mL^{-1} of $P3HT_{N_2}$ and $P3HT_{O_2}$ polymers dissolved in THF solvent. $P3HT_{N_2}$ and $P3HT_{O_2}$ were radiosynthesized in DCM respectively at 75 kGy under N_2 and at 35 kGy under O_2 atmosphere. The initial concentration of 3HT was 10 mM in both cases. Insert: photographs of the polymer powders dissolved in THF for SEC experiments.

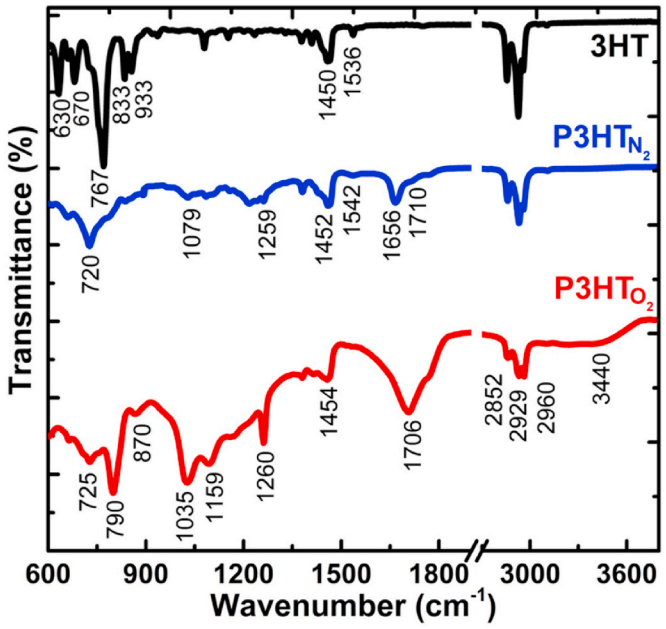

Fig. 3. ATR-FTIR spectra of pure 3HT monomers and of $P3HT_{N_2}$ and $P3HT_{O_2}$ polymers. $P3HT_{N_2}$ and $P3HT_{O_2}$ were radiosynthesized in DCM respectively at 75 kGy under N_2 and at 35 kGy under O_2 atmosphere. The initial concentration of 3HT was 10 mM in both cases.

regioregularity according to literature (Barta et al., 1999).

One can observe from SEC results that $P3HT_{O_2}$ has higher molecular weight than $P3HT_{N_2}$. In this regards, SEC's findings demonstrate that γ-induced oxidative polymerization of 3HT in dichloromethane under O_2 atmosphere not only reduces the needed irradiation dose, D_{max}, for optimal production of polymers, but also leads to P3HT materials with increased molecular weight and enlarged polymer chain. The likelihood of this slight increase is the presence of $CH_2ClO_2^{\bullet}$ and $CHCl_2O_2^{\bullet}$ peroxyl radicals produced under O_2, which afford high oxidation potential and make 3HT polymerization easier and more efficient with lower irradiation dose. In addition, the polymerization of 3HT under O_2 seemingly induces production of P3HT polymers with regioregular pattern.

3.3. Chemical characterization of $P3HT_{N_2}$ and $P3HT_{O_2}$ polymers

ATR-FTIR was used to assert the successful formation of $P3HT_{N_2}$ and $P3HT_{O_2}$ polymers in dichloromethane solutions under N_2 and O_2 atmospheres by spectral analysis of the solid parts obtained after post-processing and solvent evaporation (Scheme 2). The spectra recorded for both $P3HT_{N_2}$ and $P3HT_{O_2}$ polymers were then compared with the spectrum of pure 3HT monomers within a wavenumber region from 600 to 3600 cm^{-1} as shown in Fig. 3.

Table 1 displays the absorption modes and the positions of the representative absorption peaks of 3HT monomers, $P3HT_{N_2}$ and $P3HT_{O_2}$ polymers. The bands at 767 and 833 cm^{-1} are attributed to the = C–H out-of-plane stretching vibrations of pure 3HT monomers (Floresyona et al., 2017; Lohwasser et al., 2009) (Singh and Kaur, 2014). These peaks are remarkable in the monomer spectrum and barely noticeable in the spectra of polymers, confirming the quantitative polymerization of 3HT monomers. Of major importance, the vibration modes of the aliphatic moieties of hexyl side chain of 3HT units are observed for all samples: the asymmetric stretching vibration modes for $–CH_3$ and $–CH_2$- are detected at 2960 cm^{-1} and 2929 cm^{-1} respectively, while the symmetric -C-H stretching vibration in $–CH_2$- is detected at 2852 cm^{-1} (Floresyona et al., 2017). The peak at 720 cm^{-1} is the characteristic absorption of the in-plane and out-of-plane rocking vibration of $-(CH_2)_n-$ (Floresyona et al., 2017; Kalonga et al., 2013; Singh and Kaur, 2014). On the other hand, the symmetric C=C ring stretching vibration mode is observable for all recorded spectra around 1450 cm^{-1} (Floresyona et al., 2017; Lohwasser et al., 2009). The peaks that are assigned to asymmetrical stretching vibration modes of quinoid configuration in thiophene ring are noticeable around 1542 and 1656 cm^{-1}. Peaks at 633, 678 790, and 933 cm^{-1} are associated with the absorption of C–S–C bonds of the thiophene ring (Floresyona et al., 2017). It is worthy to note that the recorded IR spectra do not show any peak associated with C–Cl bond (Bahry et al., 2018). This proves that no chlorine atom (coming from DCM radiolysis) is covalently bonded to $P3HT_{N_2}$ and $P3HT_{O_2}$ polymer chains.

Table 1
ATR-FTIR absorption peaks of 3HT monomers and P3HT polymers.

Functional group	Position (cm^{-1})
= Cα-H (in-plane and out-of-plane deformation vibrations)	767
= Cβ-H (out-of-plane deformation vibration)	≈833
$-(CH_2)_n-$ (in-plane and out-of-plane rocking vibration)	≈ 720
C=C (symmetric stretching mode)	≈1450
C=C (asymmetrical stretching vibrations mode of quinoid configuration in thiophene ring)	1542 and 1656
C–S–C (stretching vibrations)	633, 678, 790 and 933
C=O (stretching vibrations)	≈1706
O–H (stretching vibration mode)	≈ 3100 to 3600
C–O (bending vibration)	≈ 870, 1035, 1159 and 1260

The observed peaks in the IR spectra of 3HT monomers, $P3HT_{N_2}$ and $P3HT_{O_2}$ polymers are in good agreement with 3HT and P3HT infrared spectra found in the literature (Floresyona et al., 2017; Kalonga et al., 2013). As observed in the spectrum of $P3HT_{N_2}$, a peak is very sparsely observable at 1710 cm^{-1}. This slight peak which could correspond to the signature of carbonyl groups (C=O) (Lohwasser et al., 2009) is so weak that the presence of carbonyl groups within $P3HT_{N_2}$ cannot be confirmed. The very unlikely presence of C=O bonds would be

explained in this case by the presence of traces of oxygen which could remain even after degassing. Nevertheless, as later demonstrated, no oxygen atoms were detected in $P3HT_{N_2}$ sample by EDX spectroscopy. Importantly, compared to the spectrum of $P3HT_{N_2}$, that of $P3HT_{O_2}$ is characterized by a remarkably more intense peak at around 1706 cm^{-1}, which is ascribed to C O stretching mode of the carboxylic acid group moieties (Lohwasser et al., 2009), highlighting the much more impor-tant oxidation of the polymers under O_2 atmosphere. Other specific characteristic features are also present in case of $P3HT_{O_2}$: the broad band around 3440 cm^{-1} corresponds to the vibration mode of –O-H groups interacting by hydrogen-bonds, while the prominent peaks at 870, 1035, 1159 and 1260 cm^{-1} are attributed to –C-O stretching mode (Lohwasser et al., 2009).

These observations clearly indicate that contrarily to $P3HT_{N_2}$ materials, $P3HT_{O_2}$ polymer chains are functionalized with carbonyl (-C O) and hydroxyl (-OH) moieties as well as with carboxyl (-COOH) groups. This functionalization is in good agreement with literature since successful production (according to a chemical route) of P3HT polymers functionalized with carboxylic acid groups has already been reported in literature (Lohwasser et al., 2009). This functionalization leads to hy-drophilic $P3HT_{O_2}$ polymers which can strongly interact by hydrogen-bond interactions, leading in an organic solvent such as DCM to a quantitative aggregation. This explains the formation of the sus-pended particles which are observed in insert of Fig. 1c. On the contrary, hydrophobic $P3HT_{N_2}$ polymers remain well solubilized in dichloro-methane as observed in insert of Fig. 1b, even if they can self-assemble by van der Waals interactions. This noticeable difference between $P3HT_{N_2}$ and $P3HT_{O_2}$ polymers can be explained by the differences that exist between the growth mechanisms of both polymers: first, the oxidizing species which initiate the polymerization are different ($CH_2Cl^{\bullet}$, $CHCl_2^{\bullet}$ under nitrogen on one hand and $CH_2ClO_2^{\bullet}$, $CHCl_2O_2^{\bullet}$ under oxygen on the other hand); second, while N_2 remains unreactive, O_2 molecules can react as oxidizing species. Thus, contrarily to the polymerization in an oxygen-free DCM solution which leads to non-functionalized $P3HT_{N_2}$ polymers, the polymerization in an oxygen-saturated DCM solution enables the production of oxygenated $P3HT_O$ polymers.

ATR-FTIR observations reveal the successful synthesis of P3HT polymers by both applied environmental conditions. Nevertheless, as highlighted by FTIR results, the chosen atmosphere (N_2 or O_2) has not only an influence on the yield of polymerization and on the molecular weight of the polymers but has also a clear influence on the chemical structure of the produced polymers: γ-induced polymerization in dichloromethane solvent under O_2 atmosphere is clearly advantageous if functionalized P3HT polymers are needed.

3.4. *Thermal stability analysis of $P3HT_{N_2}$ and $P3HT_{O_2}$ polymers*

Thermogravimetric analysis (TGA) was used in order to check and to compare the physicochemical properties and the thermo-degradability of $P3HT_{N_2}$ and $P3HT_{O_2}$ polymers produced in dichloromethane solvent under N_2 and O_2 atmospheres. The solid parts obtained after post- processing and solvent evaporation (Scheme 2) were used for TGA characterization.

The TGA thermograms of $P3HT_{N_2}$ and $P3HT_{O_2}$ polymers are shown in Fig. 4 $P3HT_{N_2}$ thermogram exhibits two continuous decompositions. The first one, which exhibits about 10% initial weight loss, is observed up to 110 °C. This weight loss can be attributed to the evaporation of some 3HT dimers and the degradation of the lightest 3HT oligomers. The second continuous decomposition is observed from 110 °C to 700 °C and leads to the complete degradation of the longest polymers at 700 °C. When comparing this TGA analysis with that already reported in the literature concerning P3HT polymers synthesized by conventional methodologies (Xia et al., 2014), one can note the substandard behavior of radiosynthesized $P3HT_{N_2}$ polymers, which is due to their relatively low molecular weight in comparison with that of P3HT polymers

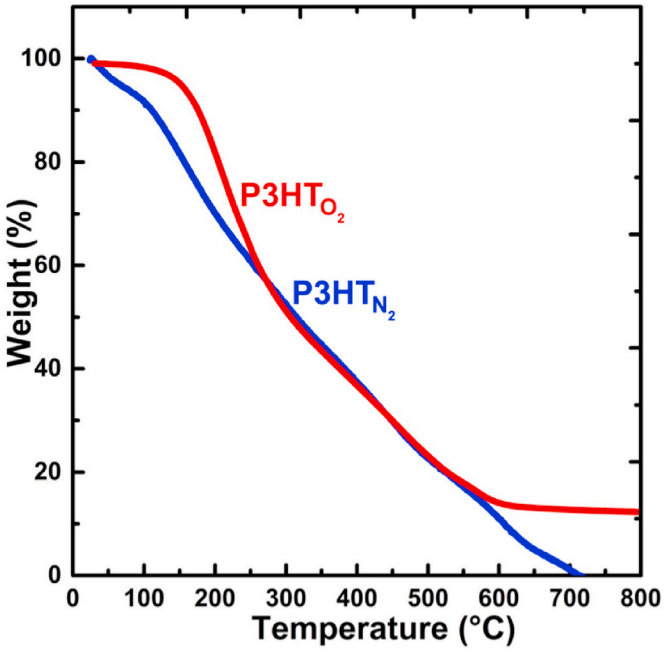

Fig. 4. Thermogravimetric analysis (TGA) graphs of dried $P3HT_{N_2}$ and $P3HT_{O_2}$ polymer powders. $P3HT_{N_2}$ and $P3HT_{O_2}$ were radiosynthesized in DCM respectively at 75 kGy under N_2 and at 35 kGy under O_2 atmosphere. The initial concentration of 3HT was 10 mM in both cases.

synthesized according to conventional routes.

In case of $P3HT_{O_2}$ TGA curve, the weight loss exhibits three stages of decomposition. Up to 155 °C, $P3HT_{O_2}$ is quite stable: only 4% of initial weight loss is detected and attributed to the degradation of oxygenated functionalities upon heating. The second decomposition is observed from 155 °C to 255 °C, which may be caused by the degradation of the smallest 3HT oligomers. The third decomposition stage, which appears continuous, is observed in the range 255–590 °C and is attributed to the degradation of longer 3HT oligomers. Importantly, $P3HT_{O_2}$ polymers with greater molecular weight (10% of the initial weight) remain stable up to 800 °C.

The present TGA findings indicate that $P3HT_{O_2}$ has better thermal stability than $P3HT_{N_2}$ at lower temperatures on the one hand and up to 800 °C on the other. This is evidently due to the higher molecular weight of $P3HT_{O_2}$ polymers as earlier highlighted by SEC analysis.

3.5. *Structural characterizations of $P3HT_{N_2}$ and $P3HT_{O_2}$ polymers*

Cryo-TEM, SEM and AFM microscopies were used in order to check and to compare the morphologies of $P3HT_{N_2}$ and $P3HT_{O_2}$ polymers produced in dichloromethane solvent at the optimal irradiation doses either under N_2 or O_2 atmospheres. For morphological characterizations, the polymers solid parts obtained after post-processing and solvent removal (Scheme 2) were once again used.

3.5.1. *Cryo-TEM observations in solution*

Thanks to sample freezing, Cryo-TEM enables *in situ* observation, into DCM solution, of radiosynthesized $P3HT_{N_2}$ and $P3HT_{O_2}$ polymers, avoiding any phase transition and any aggregation which could result from drying procedures. For this purpose, the brownish polymers powders that were obtained after post-processing were dissolved in DCM.

The captured cryo-TEM images of DCM solutions containing $P3HT_{N_2}$ or $P3HT_{O_2}$ are displayed in Fig. 5a and Fig. 5d, respectively. These two images which are representative of the two whole samples, correspond to a zoom of one of the circular holes of the holey-carbon grid coated with either $P3HT_{N_2}$ or $P3HT_{O_2}$ polymers bathing in DCM solvent. As seen

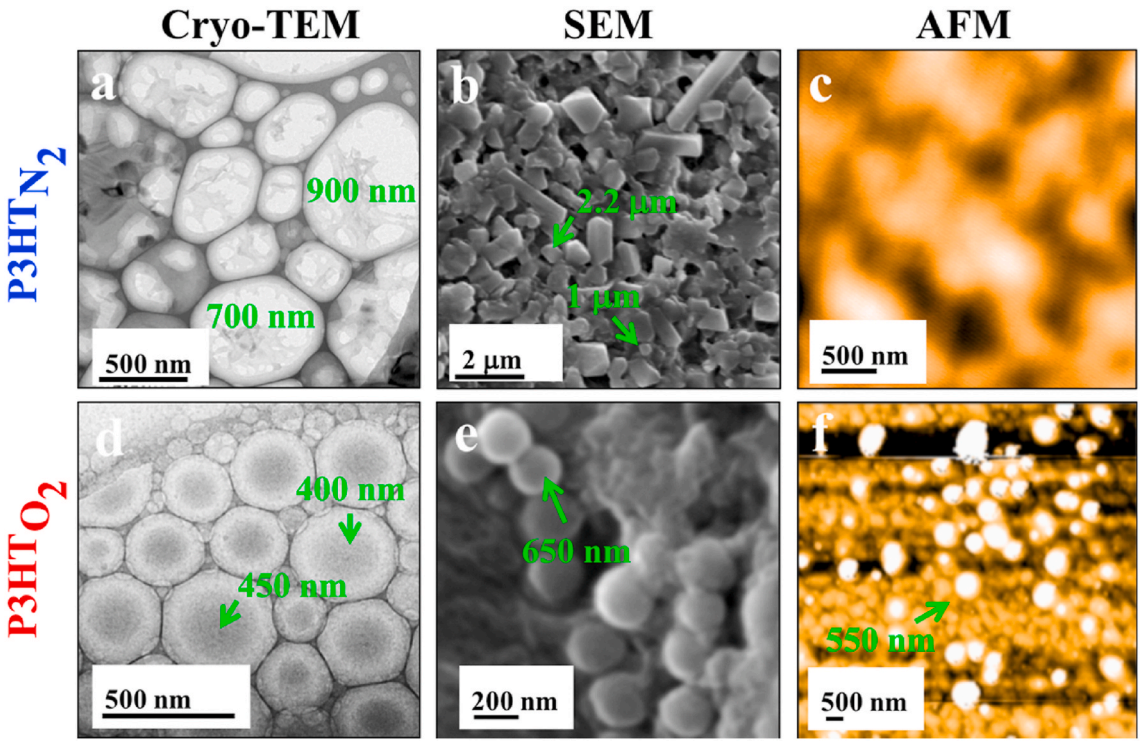

Fig. 5. Morphological characterizations of radiosynthesized $P3HT_{N_2}$ and $P3HT_{O_2}$ polymers: a) and d) Cryo-TEM images of $P3HT_{N_2}$ and $P3HT_{O_2}$ polymers self-assembled in DCM b) and e) SEM images of $P3HT_{N_2}$ and $P3HT_{O_2}$ polymer powders after deposition onto carbon tape adhered to aluminum mounts and gold coating. The powders were obtained after solvent evaporation c) and f) AFM topographic images of $P3HT_{N_2}$ and $P3HT_{O_2}$ polymers after deposition onto a mica sheet. The AFM was used in tapping mode. $P3HT_{N_2}$ and $P3HT_{O_2}$ were radiosynthesized in DCM respectively at 75 kGy under N_2 and at 35 kGy under O_2 atmosphere. The initial concentration of 3HT was 10 mM in both cases. (For interpretation of the references to color in this figure legend, the reader is referred to the Web version of this article.)

in cryo-TEM image in Fig. 5a, the hole is filled with close-packed contrasted objects. Each particle should correspond to a self-assembly of independent amorphous $P3HT_{N_2}$ polymer chains. The stones-like $P3HT_{N_2}$ particles are very heterogeneous in size and also in shape, with main sizes comprised between 100 nm and 1.5 µm. In cryo-TEM image of Fig. 5d, the circular hole of the holey-carbon grid is here also entirely full of well-contrasted objects. The observed close-packed particles, which are here made of self-assembled $P3HT_{O_2}$ polymer chains, are uniform in shape but heterogeneous in size: $P3HT_{O_2}$ particles appear as polydisperse nanospheres with diameters comprised between 50 nm and 500 nm.

As highlighted by cryo-TEM microscopy, the morphologies of $P3HT_{N_2}$ and $P3HT_{O_2}$ polymer nanoparticles are rather different. This difference in the morphology should result from the variation between the chemical structures of $P3HT_{N_2}$ and $P3HT_{O_2}$ macromolecules. Indeed, $P3HT_{N_2}$ polymers do not contain any hydrophilic oxygenated groups. As a consequence, they not only efficiently dissolve into DCM solvent (as observed in insert of Fig. 1b) but also self-assemble due to van der Waals and π-π stacking interactions, leading to stones-like $P3HT_{N_2}$ particles. Differently, $P3HT_{O_2}$ polymers are functionalized with hydrophilic carbonyl, hydroxyl and carboxyl moieties as highlighted by ATR-FTIR spectroscopy. As a consequence, their solubility in DCM solvent is poor (as observed in insert of Fig. 1c where suspended particles are observed) and their self-assembling is favored by the way of strong hydrogen-bond interactions, leading to $P3HT_{O_2}$ nanospheres. Thus, the chosen atmosphere (N_2 or O_2) which has a clear influence on the chemical structure of the synthesized P3HT polymers, also tunes the hydrophilicity and determines the morphology of the produced nanomaterials.

3.5.2. *SEM observations and EDX analysis after deposition*

SEM images were taken after deposition of dried $P3HT_{N_2}$ and $P3HT_{O_2}$ polymer powders onto carbon tape adhered to aluminum mounts and gold coating. Representative SEM images of both samples are displayed in Fig. 5b and e.

As observed in Fig. 5b, SEM image of $P3HT_{N_2}$ shows large aggregation, over several tens of micrometers, of close-packed individual blocks. These latter are heterogeneous in shape and polydisperse in size. This SEM observation agrees well with the morphology of $P3HT_{N_2}$ self-assemblies previously observed before deposition by Cryo-TEM microscopy (Fig. 5a) without any significant change neither in the mean size nor in the shape. Besides, SEM image of $P3HT_{O_2}$ is presented in Fig. 5e. It shows close-packed spherical nanoparticles with size ranging between 50 nm and several hundreds of nanometers, in good agreement with the polydisperse $P3HT_{O_2}$ nanospheres observed by Cryo-TEM before deposition (Fig. 5d). Thus, the packing of the particles and their flattening onto the substrate when deposited do not seem to affect the morphology of P3HT materials.

In order to identify the chemical composition of radiosynthesized P3HT materials and to perform the elemental analysis of the compact blocks of $P3HT_{N_2}$ (Fig. 5b) and of the aggregated nanospheres of $P3HT_{O_2}$ (Fig. 5e) in different areas of the samples, *in situ* Energy-Dispersive X-ray spectroscopy (EDX) analysis was carried out during SEM observations but without gold coating. EDX analysis highlighted the presence of both sulfur and carbon atoms in the whole $P3HT_{N_2}$ and $P3HT_{O_2}$ samples, in agreement with the chemical composition of 3HT monomers. In addition, EDX analysis enabled the detection of chlorine atoms dispersed in both $P3HT_{N_2}$ and $P3HT_{O_2}$ samples. This observation definitely proves that both radiosynthesized polymers are doped with chloride ions, as expected from DCM radiolysis and in total agreement with UV–Vis absorption spectrophotometry analysis. Interestingly, EDX spectroscopy enabled the specific detection of oxygen atoms within $P3HT_{O_2}$ sample confirming the functionalization of this kind of polymers, while oxygen atoms were not detected in $P3HT_{N_2}$ sample, in good agreement with

ATR-FTIR results.

3.5.3. AFM observations after deposition

AFM microscopy in tapping mode was used to check the topographical morphology of $P3HT_{N_2}$ and $P3HT_{O_2}$ polymers. The AFM images of $P3HT_{N_2}$ and $P3HT_{O_2}$ are exhibited in Fig. 5c and f respectively. The bottom dark areas having no thickness correspond to the substrate, while, the bright areas correspond to the topography of the samples.

The topography of $P3HT_{N_2}$ shown in Fig. 5c, displayed as the bright area, corresponds to the thicker regions made up of close aggregated polymer blocks in total agreement with cryo-TEM and SEM observations (Fig. 5a and b). The AFM topography of $P3HT_{O_2}$ presented in Fig. 5f markedly shows spheroidal nanoparticles of several hundreds of nanometers. This observation is also consistent with the recorded cryo-TEM and SEM images (Fig. 5d and e).

According to all microscopic observations (cryo-TEM, SEM and AFM), γ− radiation induced polymerization of 3HT in dichloromethane under N_2 or O_2 atmospheres leads up to two different morphologies: aggregated blocks in case of $P3HT_{N_2}$ and spheroidal nanoparticles in case of $P3HT_{O_2}$. This dissimilarity in the structure is originated from the difference in the chemical composition of the radiosynthesized polymers (while $P3HT_{N_2}$ polymers are free from any functional group, $P3HT_{O_2}$ polymers are functionalized with hydrophilic moieties) and thus results from the interaction modes between the polymer chains and with the solvent.

3.6. Examination of electrical, electrochemical and optical properties of $P3HT_{N_2}$ and $P3HT_{O_2}$ polymers

In order to investigate the physicochemical properties of $P3HT_{N_2}$ and $P3HT_{O_2}$ polymers for application opportunities in organic electronic devices such as organic photovoltaics or electrochromic devices, it is of great importance to characterize their electrical conductivity as well as their electronic and optical properties. Conductivity measurements, cyclic voltammetry experiments and Tauc's plot analysis were then used to evaluate the electrical conductivity, the electronic band gap and the optical band gap of $P3HT_{N_2}$ and $P3HT_{O_2}$ polymers produced in dichloromethane solvent at the optimal irradiation doses either under N_2 or O_2 atmospheres. The main results are listed in Table 2.

3.6.1. Conductivity measurements

After gamma-irradiation, four-point probe technique was used to measure the conductivity of $P3HT_{N_2}$ and $P3HT_{O_2}$ polymers obtained after post-processing and solvent evaporation (Scheme 2). The average electrical conductivity was calculated for both $P3HT_{N_2}$ and $P3HT_{O_2}$ samples and found equal to 0.20×10^{-3} S cm^{-1} and 0.70×10^{-3} S cm^{-1} respectively (Table 2). Even if these conductivities are much lower than the one (≈ 0.34 S cm^{-1}) reported for high molecular weight P3HT polymers chemically synthesized by $FeCl_3$ and doped with I_2 (Kuila and Nandi, 2004), radiosynthesized $P3HT_{N_2}$ and $P3HT_{O_2}$ polymers possess high conductivities when comparing to their relatively low molecular weights.

As measured, $P3HT_{O_2}$ polymer film is characterized by an electrical conductivity which is more than three times higher than that of $P3HT_{N_2}$ polymer layer (Table 2). This is a logical outcome if we consider the previous SEC data. Indeed, as earlier highlighted, $P3HT_{O_2}$ polymers have higher molecular weight and higher regioregularity degree than $P3HT_{N_2}$ materials. As a consequence, when comparing with $P3HT_{N_2}$, $P3HT_{O_2}$ conjugation length is clearly longer and its conductivity is evidently higher.

Table 2
Conductivities of $P3HT_{N_2}$ and $P3HT_{O_2}$ polymers measured by using four-point probe technique after doping with 20 mM $NOBF_4$, HOMO energy levels, LUMO energy levels and electronic band gaps calculated from cyclic voltammetry measurements and optical band gaps extrapolated from Tauc's plots. $P3HT_{N_2}$ and $P3HT_{O_2}$ polymers were radiosynthesized in DCM respectively at 75 kGy under N_2 and at 35 kGy under O_2 atmosphere. The initial concentration of 3HT was 10 mM in both cases.

Polymer	Electrical Conductivity (10^{-3} S cm^{-1})	HOMO energy level (eV)	LUMO energy level (eV)	Electronic band gap (eV)	Optical band gap (eV)
$P3HT_{N_2}$	0.20	−5.87	−3.39	2.48	2.30
$P3HT_{O_2}$	0.70	−5.87	−3.98	1.89	1.68

3.6.2. Cyclic voltammetry analysis and electrical band gap calculations

The electrochemical properties of radio-synthesized $P3HT_{N_2}$ and $P3HT_{O_2}$ polymers were further investigated by recording the corresponding cyclic voltammograms (CV) under similar experimental conditions between −2.5 V and +2.5 V (Fig. 6).

The study of cyclic voltammograms of $P3HT_{N_2}$ and $P3HT_{O_2}$ enabled the determination of oxidation, E_{ox}, and reduction, E_{red}, potentials of both polymers. CV profile of $P3HT_{N_2}$ (Fig. 6a) shows that the main p-doping (oxidation) process occurs at onset potential of +1.44 V, while n-doping (reduction) starts at −1.04 V. Moreover, CV profile of $P3HT_{O_2}$ (Fig. 6b) shows that p-doping occurs at the same onset potential of +1.44 V, while n-doping starts at a higher reduction potential: −0.45 V.

Usually, by using the equations given in caption of Fig. 6, the knowledge of E_{ox} potential value of a material enables the calculation of the energy level, E_{HOMO}, of its highest occupied molecular orbital (HOMO), while the knowledge of E_{red} potential value provides information on the energy level, E_{LUMO}, of its lowest unoccupied molecular orbital (LUMO). The calculation of the HOMO and LUMO energy levels of radiosynthesized $P3HT_{N_2}$ and $P3HT_{O_2}$ polymers was then possible (Table 2). Since $P3HT_{N_2}$ and $P3HT_{O_2}$ have the same oxidation potential, they are characterized by the same HOMO energy level: $E_{HOMO} = -5.87$ eV. However, the reduction potentials of $P3HT_{N_2}$ and $P3HT_{O_2}$ being different, their LUMO energy levels are somewhat different: $E_{LUMO} = -3.39$ eV for $P3HT_{N_2}$ and $E_{LUMO} = -3.98$ eV for $P3HT_{O_2}$. Note that E_{HOMO} and E_{LUMO} energy levels of the polymers were calculated by using the ferrocene ionization potential value as the standard (Gritzner and Kuta, 1984). Also, the corrected value of 4.8 eV vs vacuum of ferrocene is widely adopted. This value is based on the calculation obtained by Pommerehne et al. (1995).

For each kind of polymer, the knowledge of E_{HOMO} and E_{LUMO} energy levels enables the calculation of its electronic band gap: electronic band gap of $P3HT_{N_2}$ amounts to 2.48 eV when that of $P3HT_{O_2}$ is equal to 1.89

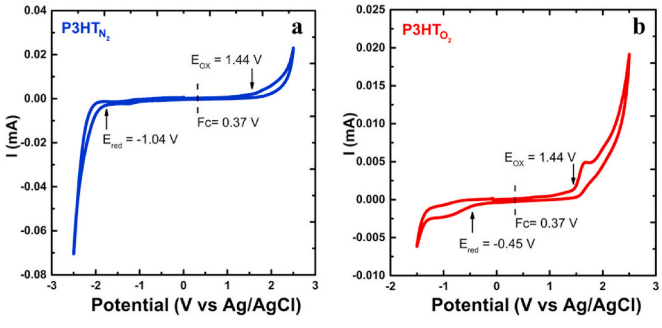

Fig. 6. Cyclic voltammograms of a) $P3HT_{N_2}$ and b) $P3HT_{O_2}$ polymers recorded in acetonitrile containing 0.1 M of $TBAPF_6$ at a scan rate of 20 mV s^{-1}. $P3HT_{N_2}$ and $P3HT_{O_2}$ were radiosynthesized in DCM respectively at 75 kGy under N_2 and at 35 kGy under O_2 atmosphere. The initial concentration of 3HT was 10 mM in both cases. Redox potential of ferrocenium/ferrocene (Fc^+/Fc) was measured to calibrate the pseudo-reference electrode (0.37 V vs. Ag/AgCl in the present study). The HOMO/LUMO energetic levels of $P3HT_{N_2}$ and $P3HT_{O_2}$ were determined as follows: E_{HOMO} (eV) from oxidation potential = - 4.8 – e (E_{ox} - 0.37) and E_{LUMO} (eV) from reduction potential = - 4.8 – e (E_{red} - 0.37) where e is the elementary charge.

eV as shown in Table 2. Interestingly, the value of the electronic band gap obtained in this work in case of radiosynthesized $P3HT_{O_2}$ polymers are in good agreement with data reported earlier on P3HT polymers synthesized by conventional methods: 1.70 eV obtained by Wu (Wu et al., 2008) and 1.96 eV by Ansari (Ansari et al., 2018).

The band gap is a major factor determining the electrical conductivity of a material. When the electronic band gap is smaller, the conductivity of the material is higher. Our energy levels calculation clearly demonstrates that electronic band gap of $P3HT_{N_2}$ polymers is larger than that of $P3HT_{O_2}$, which is in total agreement with both higher electrical conductivity (Table 2) and higher molecular weight (Fig. 2) of $P3HT_{O_2}$.

3.6.3. *Tauc's plot analysis and optical band gap calculations*

Optical band gap of a material is one more parameter which is important for applications such as in solar cells. Optical band gaps are usually deduced from Tauc's plots which are easily read out from the recorded absorption spectra of the materials. In order to draw on Tauc's plots for $P3HT_{N_2}$ and $P3HT_{O_2}$ polymers, we considered the absorption spectra of both polymers dissolved in DCM (inserts of Fig. 7a and Fig. 7b).

In the context of Tauc's plot, based on Tauc's equation applied to amorphous materials such as $P3HT_{N_2}$ and $P3HT_{O_2}$ polymers, $(\alpha h\upsilon)^{1/2}$ must be plotted as a function of photon energy ($h\upsilon$) (where α, h, υ and E_{gap} are respectively the absorption coefficient, Planck constant, light frequency, indirect optical band gap energy and A is a constant). The optical band gap, E_{gap}, can then be determined by extrapolating the straight-line portion of the Tauc's plot to photon energy axis of the plot ((Bahry et al., 2020).

As observed in Fig. 7, plotting $(\alpha h\upsilon)^{1/2}$ as a function of photon energy enabled to get the optical band gaps for both $P3HT_{N_2}$ (Fig. 7a) and $P3HT_{O_2}$ (Fig. 7b) polymers by the intercept of the two tangents to the x-axis: while optical band gap of $P3HT_{N_2}$ amounts to 2.30 eV, that of $P3HT_{O_2}$ is about 1.68 eV, as shown in Table 2. One can observe in Table 2, that for both radiosynthesized polymers, the optical band gap values (2.30 and 1.68 eV) are found smaller than the electronic ones (2.48 and 1.89 eV). This is due to the fact that measurements by electrochemistry require additional energy because of Coulomb interactions.

Tauc's plot analysis clearly demonstrates that optical band gap of $P3HT_{N_2}$ polymers is larger than that of $P3HT_{O_2}$. This difference can be understood since $P3HT_{O_2}$ possess higher molecular weight and distinct optical properties as earlier highlighted. The difference between the optical band gaps is considerable: 0.62 eV, but remains consistent with the difference between the electronic band gaps (0.59 eV).

The obtained results from electrical conductivity measurements, cyclic voltammetry experiments and optical band gaps calculations are promising and favorable for the use of both $P3HT_{N_2}$ and $P3HT_{O_2}$ polymers for practical applications. In particular, they can potentially be used in solar cells due to their appropriate and pertinent optical band gap values.

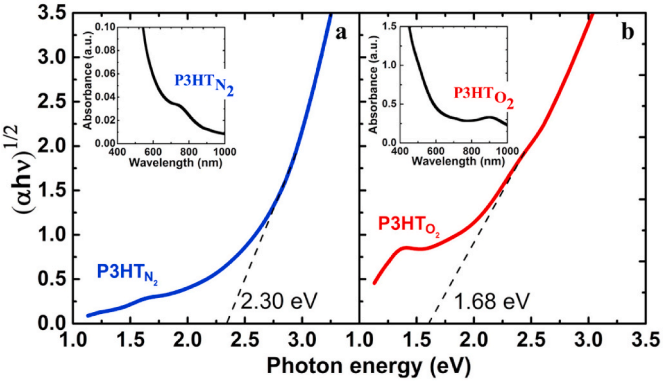

Fig. 7. Tauc's plot analysis of UV–Vis absorption spectra of a) $P3HT_{N_2}$ and b) $P3HT_{O_2}$ polymers dissolved in DCM solvent for optical band gap assessment, indicating the indirect transition for $P3HT_{N_2}$ and $P3HT_{O_2}$ materials. The UV–Vis absorption spectra of $P3HT_{N_2}$ and $P3HT_{O_2}$ dissolved in DCM are given in insert. Reference was pure sovent. L = 0.2 cm $P3HT_{N_2}$ and $P3HT_{O_2}$ were radiosynthesized in DCM respectively at 75 kGy under N_2 and at 35 kGy under O_2 atmosphere. The initial concentration of 3HT was 10 mM in both cases.

4. Conclusion

Between all conducting polymers, P3HT is considered as the best candidate for organic electronic devices, due to its good thermal stability and high processability and above all, to its remarkable optical and electronic properties. In the present study, starting from 3HT monomers which are completely insoluble in water and which are characterized by a very high redox potential, the challenge was to efficiently synthesize, by means of γ-radiolysis, nanostructured P3HT conducting polymers within dichloromethane solvent. Polymerization of 3HT into P3HT was thus conducted by following two routes: first in an oxygen-free DCM solution ($P3HT_{N_2}$) by using soft oxidizing chloromethyl ($^{\bullet}CH_2Cl$) and dichloromethyl ($^{\bullet}CHCl_2$) radicals and second in an oxygen-saturated DCM solution ($P3HT_{O_2}$) by using strong oxidizing $CH_2ClO_2^{\bullet}$ and $CHCl_2O_2^{\bullet}$ peroxyl radicals.

The various and complementary characterization methods used in the present work demonstrate the successful radiolytic synthesis of $P3HT_{N_2}$ and $P3HT_{O_2}$ conjugated polymers, which are both found doped with chloride ions generated from dichloromethane radiolysis. Due to the specific growth mechanism in an oxygen-saturated dichloromethane solution (initiation by peroxyl radicals and reactivity of O_2 molecules), $P3HT_{O_2}$ polymers are *in situ* functionalized with hydrophilic moieties, contrarily to $P3HT_{N_2}$ polymers which remain free from any functional group and thus highly hydrophobic. Such a functionalization of P3HT polymers by oxygenated moieties should improve their adhesion properties. This dissimilarity in the chemical composition of the two radiosynthesized P3HT polymers explains their different solubility behavior and the different morphologies obtained either in solution or after deposition: while $P3HT_{N_2}$ polymers self-assemble into polydisperse close-packed blocks due to van der Waals and π−π stacking interactions, $P3HT_{O_2}$ polymers form polydisperse spheroidal nanoparticles by the way of strong hydrogen-bond interactions.

The present work also highlights the advantages of using oxygen-saturated DCM solution for the production of P3HT materials with enhanced properties. First, thanks to the production of strong oxidizing agents, working under O_2 enables to increase the yield of 3HT monomers oxidation and to improve the efficiency of polymerization by reducing the irradiation dose needed for quantitative polymerization of 3HT. Secondly, γ-induced oxidative polymerization of 3HT under O_2 atmosphere leads to $P3HT_{O_2}$ materials with increased molecular weight and enlarged polymer chain, which explains the red-shift in the UV–Vis absorption spectrum of $P3HT_{O_2}$. Thirdly, thanks to the higher molecular weight and the longer conjugation length of $P3HT_{O_2}$ polymers, the materials produced under O_2 atmosphere are characterized by enhanced thermal stability, smaller optical and electronic band gaps and higher electrical conductivity.

Physicochemical properties of radiosynthesized P3HT materials, and especially those of $P3HT_{O_2}$ polymers, are quite remarkable, highlighting the success of radiation-based methodology and demonstrating that both $P3HT_{N_2}$ and $P3HT_{O_2}$ conducting polymers constitute promising candidates for different practical applications. The work is in due course in order to increase the chain length of radiosynthesized P3HT polymers produced by radiation method: by varying the dose rate or by using microreactors in order to enhance the yield of polymerization. A study in water/DCM microemulsions has started with the objective of increasing the chain length of the polymers, controlling the architecture of the produced nanomaterials and improving their optical and electrical properties. The ultimate goal clearly consists in the incorporation of

these radiosynthesized P3HT polymers in organic electronic devices such as organic photovoltaics.

CRediT authorship contribution statement

Teseer Bahry: Conceptualization, Methodology, Software, Validation, Formal analysis, Investigation, Resources, Writing - original draft, Visualization. **Zhenpeng Cui:** Investigation. **Alexandre Dazzi:** Validation, Investigation. **Matthieu Gervais:** Validation, Investigation. **Cyrille Sollogoub:** Validation, Investigation. **Fabrice Goubard:** Validation, Investigation. **Thanh-Tuân Bui:** Validation, Investigation. **Samy Remita:** Conceptualization, Methodology, Validation, Writing - original draft, Writing - review & editing, Visualization, Supervision, Project administration.

Declaration of competing interest

The authors declare that they have no known competing financial interests or personal relationships that could have appeared to influence the work reported in this paper.

Acknowledgments

We thank Jean-Michel Guigner (IMPMC, Université Pierre et Marie Curie, France) for Cryo-TEM experiments.

References

Alfassi, Z.B., Mosseri, S., Neta, P., 1989. Reactivities of chlorine atoms and peroxyl radicals formed in the radiolysis of dichloromethane. J. Phys. Chem. Us 93, 1380–1385.

Ansari, M.A., Mohiuddin, S., Kandemirli, F., Malik, M.I., 2018. Synthesis and characterization of poly(3-hexylthiophene): improvement of regioregularity and energy band gap. RSC Adv. 8, 8319–8328.

Bahry, T., Cui, Z., Deniset-Besseau, A., Gervais, M., Sollogoub, C., Bui, T.-T., Remita, S., 2018. An alternative radiolytic route for synthesizing conducting polymers in an organic solvent. New J. Chem. 42, 8704–8716.

Bahry, T., Cui, Z., Deniset, A., Gervais, M., Mbomekalle, I.M., sollogoub, C., aubet, p.-h., Bui, T.-T., Remita, S., 2020. Optimal strategy based on radiation chemistry for facile and direct synthesis of poly(3-thiophene acetic acid) polymers in water and dichloromethane. New J. Chem. 44, 11652–11666. https://doi.org/10.1039/d0nj01474e.

Barta, P., Cacialli, F., Friend, R.H., Salaneck, W.R., Zagorska, M., Pron, A., 1999. On the influence of regioregularity on electronic and optical properties of poly (alkylthiophenes). Synth. Met. 101, 296–297.

Beiting, E.J., Zeringue, K.J., Stickel, R.E., 1985. Absorption spectra of thiophene between 225 and 246 nm at elevated temperatures. Spectrochim. Acta Mol. Spectros 41, 1413–1418.

Brooke, R., Cottis, P., Talemi, P., Fabretto, M., Murphy, P., Evans, D., 2017. Recent advances in the synthesis of conducting polymers from the vapour phase. Prog. Mater. Sci. 86, 127–146.

Coletta, C., Cui, Z., Archirel, P., Pernot, P., Marignier, J.-L., Remita, S., 2015. Electron-induced growth mechanism of conducting polymers: a coupled experimental and computational investigation. J. Phys. Chem. B 119, 5282–5298.

Coletta, C., Cui, Z., Dazzi, A., Guigner, J.-M., Néron, S., Marignier, J.-L., Remita, S., 2016. A pulsed electron beam synthesis of PEDOT conducting polymers by using sulfate radicals as oxidizing species. Radiat. Phys. Chem. 126, 21–31.

Cui, Z., Bahry, T., Dazzi, A., Bui, T.-T., Goubard, F., Remita, S., 2019. Conducting polymers synthesized by γ-radiolysis in very acidic aqueous medium. Radiat. Phys. Chem. 159, 47–56.

Cui, Z., Coletta, C., Bahry, T., Marignier, J.-L., Guigner, J.-M., Gervais, M., Baiz, S., Goubard, F., Remita, S., 2017. A novel radiation chemistry-based methodology for the synthesis of PEDOT/Ag nanocomposites. Materials Chemistry Frontiers 1, 879–892.

Cui, Z., Coletta, C., Dazzi, A., Lefrançois, P., Gervais, M., Néron, S., Remita, S., 2014. Radiolytic method as a novel approach for the synthesis of nanostructured conducting polypyrrole. Langmuir 30, 14086–14094.

Cui, Z., Coletta, C., Rebois, R., Baiz, S., Gervais, M., Goubard, F., Aubert, P.-H., Dazzi, A., Remita, S., 2016. Radiation-induced reduction–polymerization route for the synthesis of PEDOT conducting polymers. Radiat. Phys. Chem. 119, 157–166.

Cutler, C., 2000. Electrochemical and Photoelectrochemical Studies of Functionalised Polythiophenes, PhD Thesis. University of Wollongong, University of Wollongong, Department of chemistry.

Emmi, S.S., Beggiato, G., Casalbore-Miceli, G., 1989. Transient species in the pulse radiolysis of methylene chloride and the self-reaction of chloromethyl radicals. Int. J. Radiat. Appl. Instrum. C Radiat. Phys. Chem. 33, 29–37.

Emmi, S.S., D'Angelantonio, M., Beggiato, G., Poggi, G., Geri, A., Pietropaolo, D., Zotti, G., 1999. The generation and spectral characterization of oligothiophenes radical cations. A pulse radiolysis investigation. Radiat. Phys. Chem. 54, 263–270.

Emmi, S.S., Poggi, G., D'Angelantonio, M., Russo, M., Favaretto, L., 2003. The solvatochromic effect on some oligothiophene radical cations: a pulse radiolysis and semiempirical investigation. Radiat. Phys. Chem. 67, 251–256.

Ferraris, J.P., Newton, M.D., 1992. Electrochemical and optical properties of thiophene-alkylheteroaromatic copolymers. Polymer 33, 391–397.

Floresyona, D., Goubard, F., Aubert, P.-H., Lampre, I., Mathurin, J., Dazzi, A., Ghosh, S., Beaunier, P., Brisset, F., Remita, S., Ramos, L., Remita, H., 2017. Highly active poly (3-hexylthiophene) nanostructures for photocatalysis under solar light. Appl. Catal. B Environ. 209, 23–32.

Gritzner, G., Kuta, J., 1984. Recommendations on reporting electrode potentials in nonaqueous solvents. Pure Appl. Chem. 56, 461–466.

Ishigaki, A., Koizumi, H., 2012. Radiation-induced polymerization of 3-octylthiophene. Radiat. Phys. Chem. 81, 803–806.

Isse, A.A., Lin, C.Y., Coote, M.L., Gennaro, A., 2011. Estimation of standard reduction potentials of halogen atoms and alkyl halides. J. Phys. Chem. B 115, 678–684.

Jiang, C., Chen, G., Wang, X., 2012. High-conversion synthesis of poly(3,4-ethylenedioxythiophene) by chemical oxidative polymerization. Synth. Met. 162, 1968–1971.

Kalonga, G., Chinyama, K., Munyati, O., Maaza, M., 2013. Characterization and Optimization of P3HT and PCBM Blends for Photo-Absorption.

Kim, T., Kim, J., Kim, Y., Lee, T., Kim, W., Suh, K.S., 2009. Preparation and characterization of poly(3,4-ethylenedioxythiophene) (PEDOT) using partially sulfonated poly(styrene-butadiene-styrene) triblock copolymer as a polyelectrolyte. Curr. Appl. Phys. 9, 120–125.

Kuila, B.K., Nandi, A.K., 2004. Physical, mechanical, and conductivity properties of poly (3-hexylthiophene)−Montmorillonite clay nanocomposites produced by the solvent casting method. Macromolecules 37, 8577–8584.

Lattach, Y., Coletta, C., Ghosh, S., Remita, S., 2014. Radiation-induced synthesis of nanostructured conjugated polymers in aqueous solution: fundamental effect of oxidizing species. ChemPhysChem 15, 208–218.

Lattach, Y., Deniset-Besseau, A., Guigner, J.-M., Remita, S., 2013. Radiation chemistry as an alternative way for the synthesis of PEDOT conducting Polymers under "soft" Conditions. Radiat. Phys. Chem. 82, 44–53.

Lohwasser, R.H., Bandara, J., Thelakkat, M., 2009. Tailor-made synthesis of poly(3-hexylthiophene) with carboxylic end groups and its application as a polymer sensitizer in solid-state dye-sensitized solar cells. J. Mater. Chem. 19, 4126–4130.

Marrocchi, A., Lanari, D., Facchetti, A., Vaccaro, L., 2012. Poly(3-hexylthiophene): synthetic methodologies and properties in bulk heterojunction solar cells. Energy Environ. Sci. 5, 8457–8474.

Mccullough, R.D., Tristramnagle, S., Williams, S.P., Lowe, R.D., Jayaraman, M., 1993. Self-orienting head-to-tail poly(3-alkylthiophenes) - new insights on structure-property relationships in conducting polymers. J. Am. Chem. Soc. 115, 4910–4911.

Murali, M.G., Rao, A.D., Yadav, S., Ramamurthy, P.C., 2015. Narrow band gap conjugated polymer for improving the photovoltaic performance of P3HT:PCBM ternary blend bulk heterojunction solar cells. Polym. Chem. 6, 962–972.

Pappenfus, T.M., Hermanson, D.L., Kohl, S.G., Melby, J.H., Thoma, L.M., Carpenter, N.E., da Silva Filho, D.A., Bredas, J.-L., 2010. Regiochemistry of poly(3-hexylthiophene): synthesis and investigation of a conducting polymer. J. Chem. Educ. 87, 522–525.

Pommerehne, J., Vestweber, H., Guss, W., Mahrt, R.F., Bässler, H., Porsch, M., Daub, J., 1995. Efficient two layer leds on a polymer blend basis. Adv. Mater. 7, 551–554.

Roncali, J., Garreau, R., Yassar, A., Marque, P., Garnier, F., Lemaire, M., 1987. Effects of steric factors on the electrosynthesis and properties of conducting poly(3-alkylthiophenes). J. Phys. Chem. 91, 6706–6714.

Singh, B., Kaur, A., 2014. Photoelectrical, optical, and transport properties of poly (3-hexylthiophene)-zinc sulfide hybrid nanocomposites. J. Appl. Phys. 116, 063709.

Tremel, K., Ludwigs, S., 2014. Morphology of P3HT in thin films in relation to optical and electrical properties. In: Ludwigs, S. (Ed.), P3HT Revisited – from Molecular Scale to Solar Cell Devices. Springer Berlin Heidelberg, Berlin, Heidelberg, pp. 39–82.

Truszkowski, S., Szymański, W., 1994. Stable products and radicals in the radiolysis of dichloromethane and 1,1,-dichloroethane gamma-irradiated in an oxygen-free atmosphere. J. Radioanal. Nucl. Chem. 177, 415–423.

Ushida, K., Yoshida, Y., Kozawa, T., Tagawa, S., Kira, A., 1999. Evidence of oxidation of aromatic hydrocarbons by chloromethyl Radicals: reinvestigation of intersolute hole transfer using pulse radiolysis. J. Phys. Chem. 103, 4680–4689.

Wei, Y., Chan, C.C., Tian, J., Jang, G.W., Hsueh, K.F., 1991. Electrochemical polymerization of thiophenes in the presence of bithiophene or terthiophene: kinetics and mechanism of the polymerization. Chem. Mater. 3, 888–897.

Wu, I.C., Lai, C.-H., Chen, D.-Y., Shih, C.-W., Wei, C.-Y., Ko, B.-T., Ting, C., Chou, P.-T., 2008. Cu(i) chelated poly-alkoxythiophene enhancing photovoltaic device composed of a P3HT/PCBM heterojunction system. J. Mater. Chem. 18, 4297–4303.

Xia, H., Ye, Z., Liu, X., Peng, J., Qiu, F., 2014. Synthesis, characterization, and solution structure of all-conjugated polyelectrolyte diblock copoly(3-hexylthiophene)s. RSC Adv. 4, 19646–19653.